ISSN 1069-3513, Izvestiya, Physics of the Solid Earth, 2008, Vol. 44, No. 10, pp. 789–803. © Pleiades Publishing, Ltd., 2008.
Original Russian Text © A.F. Grachev, D.M. Pechersky, S.E. Borisovskii, V.A. Tselmovich, 2008, published in Fizika Zemli, 2008, No. 10, pp. 40–55.

Magnetic Minerals in Sediments at the Cretaceous/Paleogene Boundary (the Gams Section, Eastern Alps)

A. F. Grachev[a], D. M. Pechersky[a], S. E. Borisovskii[b], and V. A. Tselmovich[a]

[a] *Schmidt Institute of Physics of the Earth, Russian Academy of Sciences (RAS), Bol'shaya Gruzinskaya ul. 10, Moscow, 123995 Russia (e-mail: afgrachev@gmail.com)*

[b] *Institute of Geology of Ore Deposits, Petrography, Mineralogy, and Geochemistry (IGOD), RAS, Staromonetnyi per. 35, Moscow, 119017 Russian Federation (e-mail: bor@igem.ru)*

Received March 30, 2008

Abstract—The paper presents results of detailed magnetomineralogical and microprobe studies of sediments at the Cretaceous/Paleogene (K/T) boundary in two epicontinental sections in the Eastern Alps (Austria), where deposits, including the K/T boundary, outcrop along the Gams River and its tributaries. K/T boundary layers in these sections are similar in the set of such magnetic minerals as iron hydroxides, ferrospinels, hemoilmenite, titanomagnetite, magnetite, hematite, and metallic iron. However, the boundary layer in the Gams-1 section is distinguished by the presence of metallic nickel and its alloy with iron and by the absence of iron sulfides, whereas nickel has not been discovered in the Gams-2 section, which, however, contains iron sulfides of the pyrite type. Therefore, these minerals occur locally. It is suggested that enrichment in iron hydroxides of a common origin can be regarded as a global phenomenon inherent in the K/T boundary and unrelated to an impact event.

PACS numbers: 91.25.Ng

DOI: 10.1134/S1069351308100078

1. INTRODUCTION

This paper belongs to a cycle of magnetomineralogical and microprobe studies of sediments at the Mesozoic/Cenozoic (K/T) boundary and is devoted to a detailed layerwise study of the K/T boundary layer in epicontinental deposits outcropping along the Gams River and its tributaries near the village of Gams (Eastern Alps) [Lahodynsky, 1988; Grachev et al., 2005]. Samples were collected in the Gams-1 and Gams-2 outcrops ~0.5 km apart.

We should emphasize that, in all of the previously studied sections [Pechersky, 2008], the boundary layer is distinguished by an anomalous peak of the paramagnetic magnetization and magnetic susceptibility related to the high overall concentration of iron present primarily in both paramagnetic and weakly ferromagnetic (goethite) hydroxides; i.e., beginning from the boundary layer, an abrupt jump in the iron accumulation in sediments takes place. The observed positive correlation ($K \approx 0.9$) between the goethite concentration and the paramagnetic susceptibility implies that the paramagnetic material primarily consists of Fe hydroxides.

2. METHODS OF STUDY

Thermomagnetic analysis (TMA) was applied to rock samples. To estimate the concentration of magnetic minerals in the samples, TMA curves were used to determine the contribution of a magnetic mineral with a given Curie point to the sample magnetization, and this value was divided by the specific saturation magnetization of this mineral: 90 A m^2/kg for magnetite and titanomagnetite, 200 A m^2/kg for iron, 4 A m^2/kg for hemoilmenite with $T_C > 300$°C, 10 A m^2/kg for hemoilmenite with $T_C \approx 250$–260°C, and 0.25 A m^2/kg for goethite. Pyrite and arsenopyrite grains are noted in Gams-2 boundary layer clay samples. Upon heating, such minerals are oxidized and magnetite forms and, using the amount of the newly-formed magnetite, we obtain an approximate estimate (a lower bound) of the concentration of Fe sulfides of the pyrite and arsenopyrite type.

The paramagnetic magnetization of samples was determined using the relation $M_p = 1.378(M_{20} - M_{800})$, where M_{20} is the "total," paramagnetic+diamagnetic magnetization of the sample determined from the curve of its isothermal magnetization at room temperature above the saturation field of magnetic minerals present in the sample, and M_{800} is the sample magnetization value obtained at 800°C in the same field as M_{20}.

Along with petromagnetic investigations, magnetic minerals in thin sections and in heavy and magnetic fractions extracted from sediments were analyzed with the use of Camebax and Tescan Vega microprobes. The extracted particles were cleaned with ultrasound and

Table 1. Composition of titanomagnetite grains in the boundary layer of the Gams section

(a) Gams-1

Grain	Layer	TiO_2	FeO*	MgO	CaO	MnO	Cr_2O_3	Al_2O_3
1	$J6_1$	23.0	72.2	0.1	–	0.1	–	0.1
2	$J6_1$	20.8	74.9	0.1	–	0.2	–	0.2
3	$J6_2$	22.2	73.1	0.2	–	0.2	–	0.1
4	Bottom	13.76	75.93	–	–	0.04	–	–
5	″	8.79	80.38	–	–	–	0.04	–
6	″	13.06	76.93	–	–	–	0.07	–
7	Middle	15.97	75.39	0.08	–	0.12	0.07	–
8	″	12.30	78.54	0.08	–	–	0.04	–
9	″	13.73	77.02	–	–	0.16	0.07	–
10	″	15.13	75.54	–	–	0.07	0.09	–
11	Top	14.63	76.92	0.08	–	0.40	0.12	–
12	″	9.41	81.03	–	–	–	0.13	–
13	″	14.56	75.97	0.08	–	0.17	–	0.11
14	″	15.06	77.21	–	–	0.04	0.07	–
15	″	10.32	81.55	–	–	–	0.06	–

(b) Gams-2

Grain	Layer	TiO_2	FeO*	MgO	CaO	MnO	Cr_2O_3	Al_2O_3	SiO_2	NiO
16	2	10.88	79.71	0.03	0.01	0.35	0.11	0.06	0.02	0.02
17	2	12.46	78.06	0.00	0.00	0.37	0.10	0.05	0.00	0.00
18	2	34.54	58.28	0.01	0.01	0.00	0.26	0.06	0.00	0.01
19	2	15.17	75.67	0.04	0.00	0.25	0.06	0.04	0.03	0.00
20	2	13.09	77.13	0.05	0.01	0.38	0.08	0.01	0.00	0.00
21	2	16.43	74.44	0.03	0.01	0.00	0.32	0.01	0.01	0.00
22	3	14.46	75.90	0.02	0.01	0.00	0.15	0.10	0.00	0.00
23	3	11.74	79.72	0.07	0.01	0.29	0.08	0.05	0.00	0.06
24	3	13.41	77.24	0.03	0.00	0.00	0.10	0.10	0.00	0.01
25	3	15.01	74.08	0.02	0.01	0.03	0.13	0.11	0.00	0.00
26	3	20.66	71.58	0.04	0.02	0.28	0.12	0.06	0.02	0.00
27	3	12.58	77.84	0.03	0.00	0.16	0.09	0.06	0.01	0.04
28	3	15.79	74.92	0.03	0.01	0.17	0.17	0.06	0.01	0.01
29	3	13.43	76.40	0.03	0.00	0.00	0.15	0.08	0.05	0.00
30	3	11.37	79.36	0.00	0.01	0.12	0.19	0.12	0.02	0.00
31	3	15.12	75.84	0.05	0.00	0.21	0.10	0.05	0.00	0.03
32	3	14.05	76.51	0.00	0.01	0.14	0.10	0.02	0.01	0.00
33	3	8.73	80.46	0.00	0.02	0.01	0.20	0.10	0.02	0.02
34	3	15.72	74.18	0.00	0.01	0.01	0.21	0.08	0.00	0.02
35	4	13.50	77.93	0.00	0.02	0.03	0.26	0.12	0.01	0.05
36	4	11.06	79.98	0.04	0.01	0.05	0.12	0.06	0.00	0.00
37	4	32.31	60.00	0.00	0.00	1.05	0.03	0.02	0.01	0.00
38	4	13.88	76.77	0.04	0.01	0.04	0.09	0.10	0.00	0.01
39	4	13.81	77.64	0.04	0.02	0.17	0.03	0.00	0.03	0.01
40	4	14.04	76.66	0.03	0.03	0.23	0.07	0.07	0.07	0.01
41	4	29.38	66.71	0.01	0.01	0.42	0.04	0.00	0.00	0.00
42	4	13.73	77.05	0.01	0.00	0.10	0.10	0.10	0.03	0.00

Note: 1–3, heavy fraction from Gams-1A; 4–15, heavy fraction from Gams-1B; 16–42, heavy fraction from Gams-2B. In all tables, the asterisk means that all the iron is reduced to FeO.

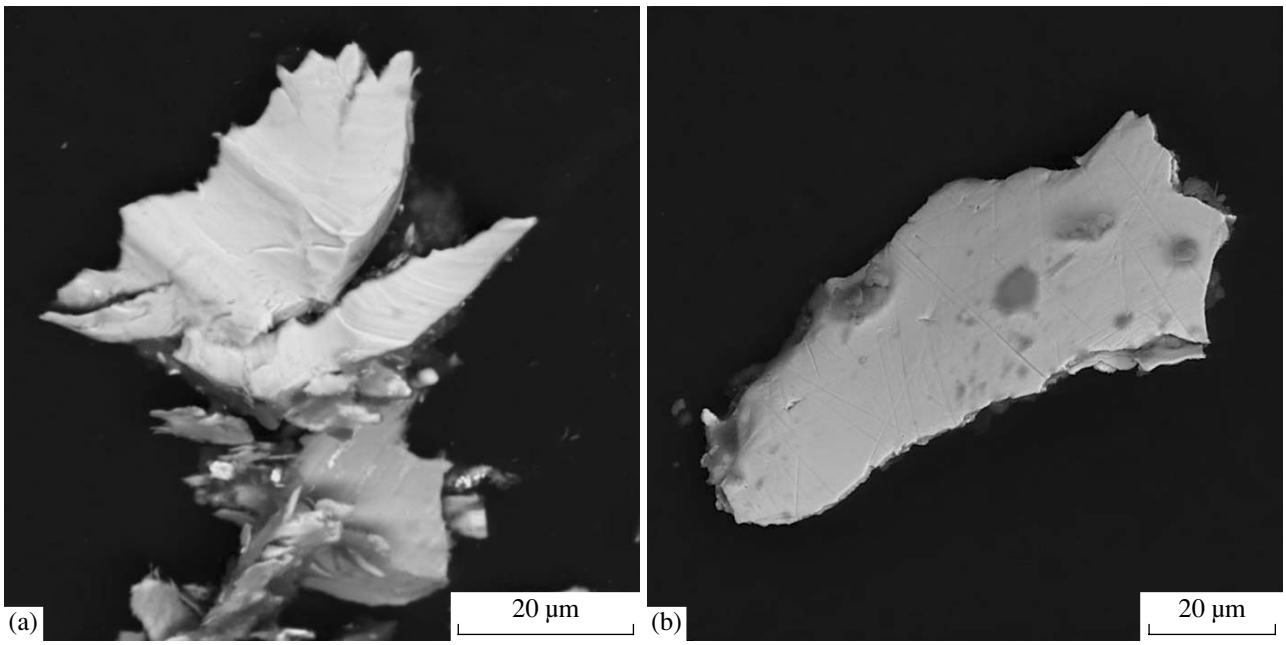

Fig. 1. Examples of flaky particles of metallic nickel (Gams-1B).

etched with hydrochloric acid. Using a strong constant magnet, the fraction material was fixed on a conductive film with a bilateral adhesive layer. The effective diameter of the microprobe was about 2 μm. Microprobe measurements were made with an accelerating voltage of 20 kV and a beam current of 10 nA.

On the whole, the results of microprobe and thermomagnetic analyses are complementary. For example, (a) a divergence between titanomagnetite compositions determined from the microprobe and thermomagnetic data is evidence for a fine decomposition of titanomagnetite grains and (b) the fact that nickel is discovered in the magnetic fraction of some samples from the microprobe study but is absent there according to MTA data, and vice versa, suggests a local and very nonuniform distribution of Ni particles. We should note that 10–20 g of material were taken to obtain heavy and magnetic fractions, whereas a sample ~0.1 g in weight was taken for the TMA; i.e., the probability of detecting individual grains of magnetic minerals in a sample by the TMA method is two orders smaller compared to the examination of a heavy and/or magnetic fraction.

We examined four hand samples from clay boundary layers of the following sections: the Gams-1A layer ~2 cm thick, samples from six levels were studied; the Gams-1B, samples from five levels; the Gams-2A layer ~5 cm thick, samples from nine levels; and the Gams-2B layer ~4 cm thick, samples from five levels.

3. RESULTS OF STUDIES

Here, we briefly describe results of thermomagnetic and microprobe studies of magnetic minerals in all deposits of the Gams-1 section [Grachev et al., 2005; Pechersky et al., 2006]. (1) Weakly ferromagnetic iron hydroxides of the goethite type (T_C = 90–150°C) vary along the section from 0.5% in Maastrichtian limestones to 2–2.5% in the boundary layer and Danian sandy–clayey sediments. (2) Hemoilmenite of variable composition (T_C = 180–300°C) is present in all samples. The heavy and magnetic fractions contain numerous ilmenite grains. Fine segregations of hemoilmenite, a product of multiphase oxidation of ilmenite, are observed in ilmenite grains. (3) Metallic nickel (T_C = 350–370°C) is found in the $J6_6$ and $J6_4$ samples of the boundary layer. (4) Titanomagnetite and magnetite (T_C = 550–610°C) are present in all section samples studied. Most of the titanomagnetite is altered up to magnetite due to multiphase oxidation. After heating, this phase is generally preserved, but its amount commonly decreases and T_C shifts leftward; i.e., as a result of heating to 800°C, titanomagnetite grains are partially homogenized and partially destroyed (oxidizing to hematite). The former feature is used as a diagnostic criterion of titanomagnetite. According to microprobe data, the grains are close in composition to basalt titanomagnetites (TiO_2 ~ 20–25%). (5) An Fe–Ni alloy (taenite) (T_C = 640–660°C) is present in boundary layer samples and sample *L*6 from Danian deposits. (6) Metallic iron with minor admixtures (T_C = 740–770°C) is present in the majority of Gams horizons. Metallic iron is almost absent in the boundary layer according to TMA data, while its isolated grains are found in the magnetic fraction of the K/T layer.

The boundary clay layer *J*6 (Gams-1A) can be characterized as follows (from bottom to top).

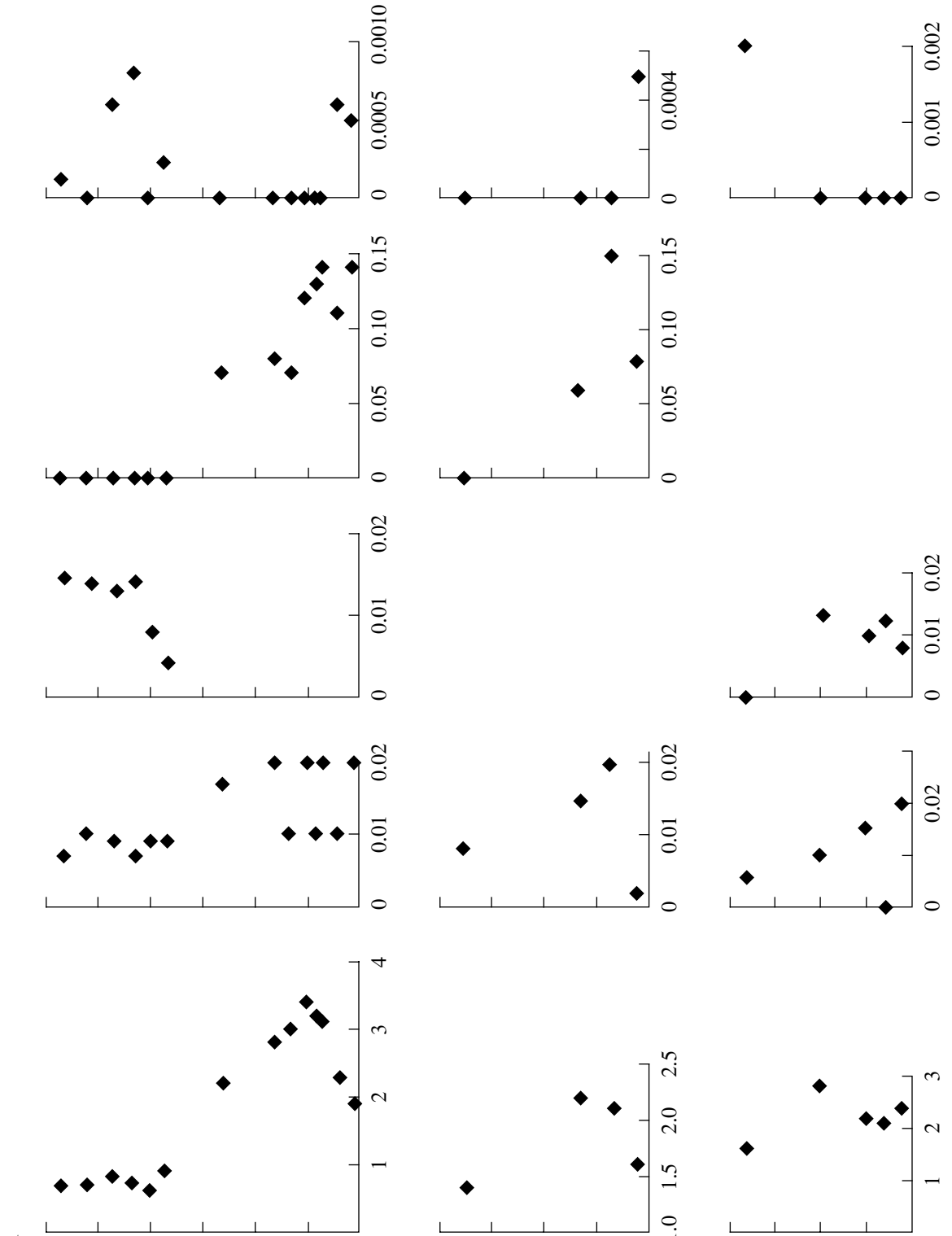

Fig. 2. Percentage concentrations of goethite, titanomagnetite, magnetite, "pyrite" (amount of magnetite formed from "pyrite" during laboratory heating of a sample), and metallic iron in the Gams-2A, Gams-2B, and Gams-1B sections from TMA data.

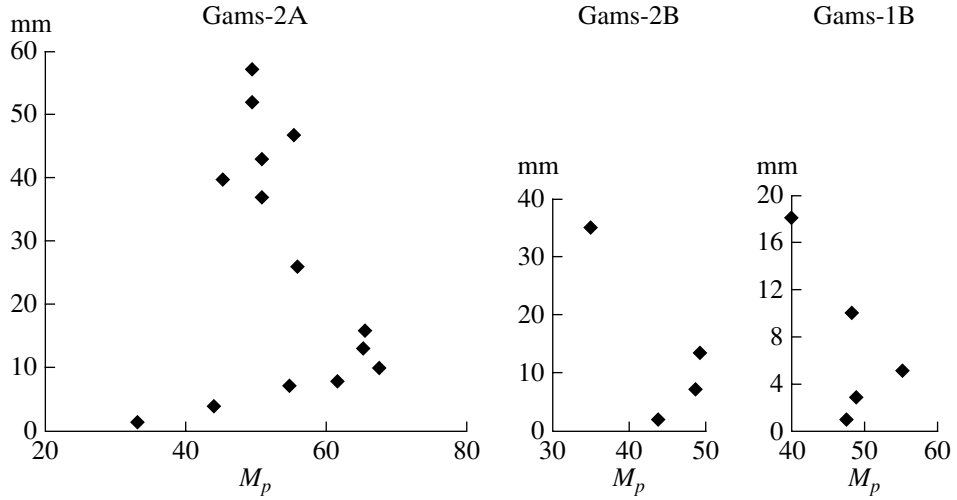

Fig. 3. Paramagnetic magnetization M_p (10^{-3} A m^3/kg) in the boundary layer and overlying sediments (Gams-2A, Gams-2B, and Gams-1B).

J6$_1$. According to TMA data, the sample contains ~0.2% titanomagnetite with T_C = 540°C. The microprobe study discovered grains of titanomagnetite and ilmenite, occasionally as intergrowths. The composition of the titanomagnetite grains (TiO_2 ~ 0.2–0.23%, Table 1) is at variance with the Curie point, implying that the grains were subjected to multiphase oxidation and decomposition. During heating, a part of fine grains of magnetite and titanomagnetite is oxidized to hematite, as is evident from a sharp drop of the magneti-

Table 2. Composition of hydrogoethite from the Gams-2B boundary layer

FeO*	SiO_2	NiO	CaO	MnO	Al_2O_3	Cr_2O_3	MgO	TiO_2	Total
68.54	1.98	0.00	0.25	0.02	1.18	0.17	0.01	0.00	72.13
67.09	0.03	0.00	0.74	0.00	3.08	0.00	0.00	0.03	70.97
65.58	0.00	0.02	0.74	0.01	3.08	0.00	0.00	0.00	69.43
65.30	0.02	0.02	0.74	0.00	3.10	0.02	0.00	0.00	69.20
59.72	7.25	1.35	0.15	4.45	0.09	0.08	0.03	0.00	73.12

Table 3. Examples of altered ilmenites (hydration, iron removal, etc.) from the Gams-2 boundary layer

FeO*	MnO	TiO_2	MgO	NiO	Cr_2O_3	SiO_2	Al_2O_3	CaO	Total
32.32	0.28	58.24	0.00	0.00	0.00	0.39	0.00	0.06	91.29
36.79	1.21	51.55	0.00	0.00	0.04	0.15	0.02	0.03	89.79
49.36	1.43	45.71	0.13	0.00	0.03	0.06	0.00	0.01	96.73
42.12	2.17	53.24	0.10	0.00	0.00	0.06	0.00	0.00	97.69
38.34	2.63	55.64	0.07	0.00	0.00	0.15	0.08	0.01	96.92
36.38	1.78	55.82	0.00	0.00	0.00	0.32	0.02	0.06	94.38

Table 4. Composition of magnetite from the transitional layer f the Gams-1A section

Element	1	2	3	4	5	6	7	8	9	10
TiO_2	1.11	–	–	–	–	0.03	0.27	–	–	–
FeO*	98.89	93.17	97.92	93.1	92.9	98.77	87.76	99.46	99.68	99.28
MgO	–	–	–	0.1	0.4	0.05	1.79	–	–	–
MnO	–	–	–	0.2	0.1	0.08	0.08	0.54	–	0.72
Al_2O_3	–	6.83	2.08	0.1	0.4	0.11	–	–	0.32	–
Cr_2O_3	–	–	–	0.1	–	–	9.13	–	–	–
NiO	–	–	–	–	–	0.08	1.16	–	–	–
Element	11	12	13	14	15	16	17	18	19	20
TiO_2	–	–	–	–	–	–	–	–	–	–
FeO	97.73	96.50	96.91	98.05	98.34	97.73	89.87	91.10	89.87	91.07
MgO	–	–	–	–	–	–	5.83	3.49	5.83	3.52
MnO	0.83	1.02	0.75	0.79	0.71	0.83	0.59	–	0.59	–
Al_2O_3	1.45	2.48	1.56	1.16	0.95	1.45	–	0.72	–	0.72
Cr_2O_3	–	–	–	–	–	–	1.65	2.44	1.65	2.44
NiO	–	–	–	–	–	–	2.06	2.25	2.06	–
CuO	–	–	0.77	–	–	–	–	–	–	–

Note: 1–3, Gams-1A transitional layer (thin section); 4–5, heavy fraction from the middle part of the Gams-1A transitional layer; 6–20, heavy fraction from the middle part of the Gams-1B transitional layer. Unfilled cells correspond to concentrations below the microprobe sensitivity threshold.

Table 5. Composition of magnetite from magnetic fractions of Danian sediments in the Gams-1 section

Sample, grain	TiO_2	FeO*	MgO	MnO	Al_2O_3	Cr_2O_3
L6, 7	0.0	93.8	0.1	0.2	0.1	0.0
8	0.0	93.8	0.2	0.1	0.1	0.1
L7, 1	0.0	93.9	0.0	0.0	0.5	0.1
M4, 1	0.0	93.1	0.0	0.1	0.1	0.0
2	0.0	95.2	0.0	0.2	0.2	0.0
4	0.0	93.9	0.1	0.1	0.1	0.0
O4/5, 1	0.0	94.1	0.0	0.0	0.2	0.1
2	0.0	95.2	0.0	0.2	0.2	0.0
5	0.0	93.6	0.0	0.1	0.1	0.1
7	0.0	94.6	0.2	0.0	0.2	0.1
P5,6 2	0.0	94.2	0.2	0.1	0.1	0.0
3	0.0	93.9	0.0	0.2	0.3	0.1

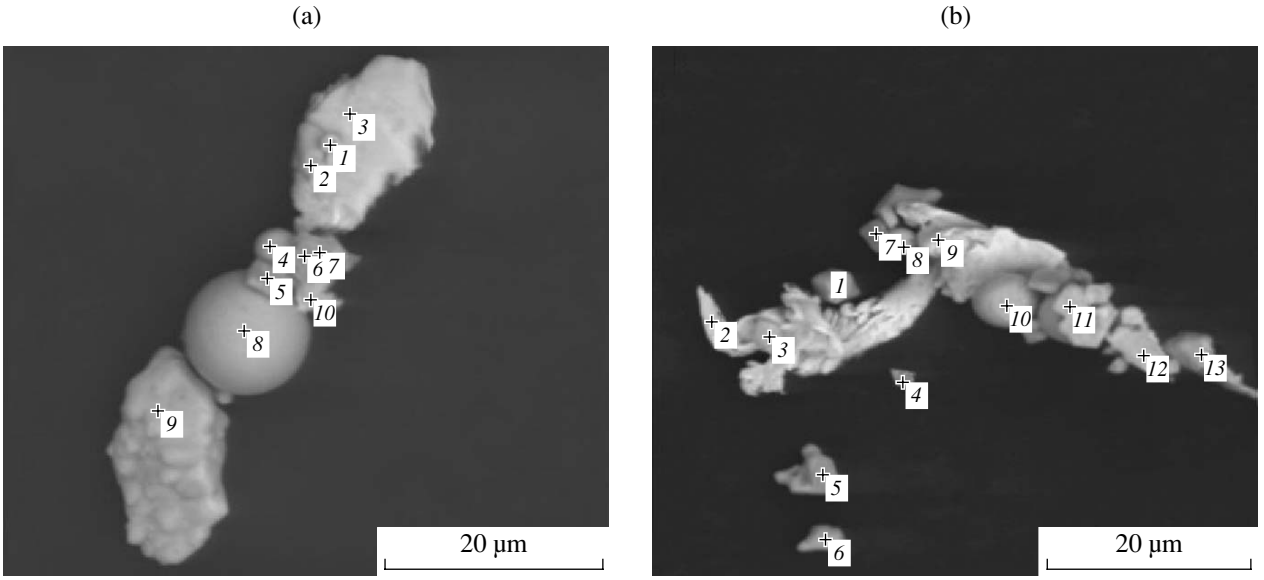

Grain	O	Mg	Al	Si	Cr	Mn	Fe	Ni	Cu
1	28.65	7.70	1.92	0.52	5.32	1.12	53.14	1.64	
2	3.93		0.47		0.39		94.31		0.90
3							100.00		
4	39.47	1.35	0.53		0.58	1.10	50.14	6.85	
5	33.16						66.84		
6, 7	27.47	4.57	3.66	3.14	4.60		51.88	4.67	
8	26.64		0.42				72.94		
9	30.88		0.37				68.75		
10	3.28						96.72		

Grain	O	Mg	Al	Si	Ca	Ti	Cr	Mn	Fe	Ni
1	35.72	6.08	1.20				3.52	1.05	46.82	4.91
2	3.47						0.29		96.24	
3	33.97	3.71	2.31	0.26			8.43	1.10	46.57	3.65
4	18.72						2.76	0.98	73.34	4.20
5	35.13	5.00	1.83	0.56		0.29	6.49	0.56	45.95	4.19
6	29.55	4.71	1.71				9.20	0.67	49.59	4.56
7	38.49	5.72	1.96		0.20	0.24	4.73	0.62	44.08	3.96
8	32.21								67.79	
9								0.68	99.32	
10	30.58			0.35					69.07	
11	29.99	1.36	0.40	0.25	0.33		0.81	1.05	59.83	5.98
12	5.45	0.91		0.68	0.71			0.52	90.51	
13	9.75				0.65			0.48	88.44	0.68

Fig. 4. Lower part of the Gams-2B boundary layer. (a) Examples of particles from the magnetic fraction: metallic iron (*2–3*, *10*), magnetite ball (*8*), Ni-bearing ferrospinel (*1*, *4*, *7*), and hematite from magnetite (*5*, *9*). The Ni-bearing ferrospinel grain (*1*) is included in the particle of metallic iron (*2, 3*), which is evidence for the cosmic origin of the ferrospinel crystal. (b) Examples of particles from the magnetic fraction: metallic iron (*2*, *9*, *12*, *13*), balls of hematite from iron (*8*, *10*), and Ni-bearing ferrospinel (*1*, *3–7*, *11*). (c) A large "caterpillar" of partially oxidized metallic iron (*3*), small lamellae of Ni–Fe–Mo alloy (*7*, *8*, *10*), and fine crystals of ferrospinel (*2*, *4*, *5*, *6*). (d) A lamella of metallic iron (*5*, *6*, *7*), fine crystals of Ni-bearing ferrospinel (*1–3*), and a hematite ball (*4*).

zation after the first heating to 700°C, while other grains are partially homogenized (with a leftward shift of the Curie point to 510°C after the first heating), which also leads to a drop in the magnetization. Maghemite is noted in nearly all laminae of the Gams-1A section. Its fraction relative to the titanomagnetite content is ~10%.

J6$_2$. TMA data point to the presence of ~0.002% of magnetite with T_C ~ 570°C and ~0.2% of hemoilmenite with $T_C \approx 270$°C; a microprobe detected a metallic iron ball. Very fine grains of titanomagnetite (from fractions of a micrometer to a few micrometers) are present; they could not be correctly diagnosed. The concentration of magnetic minerals is about 20 times lower as compared with the sublayer $J6_1$.

J6$_3$. According to TMA data, the sample contains titanomagnetite with the Curie point T_C ~ 500°C shifting to 480°C due to partial homogenization and magnetite with T_C = 590°C. As in $J6_2$, the concentration of magnetic minerals is significantly lower than in $J6_1$: ~0.01% titanomagnetite and ~0.003% magnetite. The microprobe data point to the presence of magnetite and ilmenite particles more than 10 μm in size and numerous finer particles of magnetite.

J6$_4$. According to TMA data, metallic nickel with T_C = 350°C (~0.005%), magnetite with T_C = 590°C (~0.002%), and iron with T_C > 730°C are present. A microprobe fixed lamellae of metallic nickel in the magnetic fraction (Fig. 1).

(c)

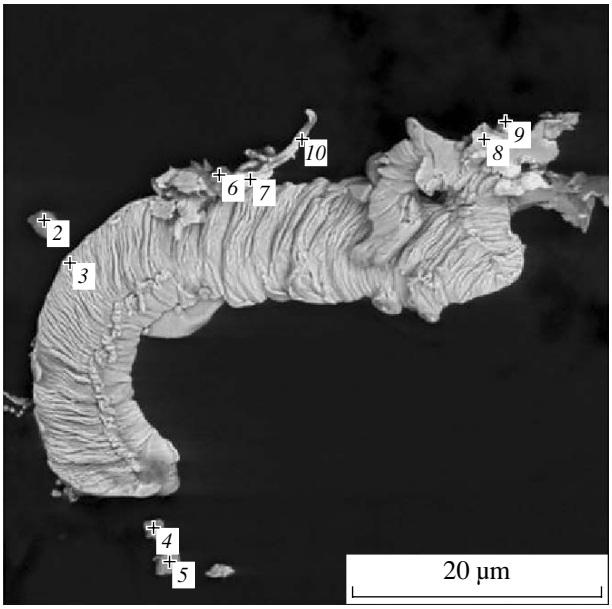

(d)

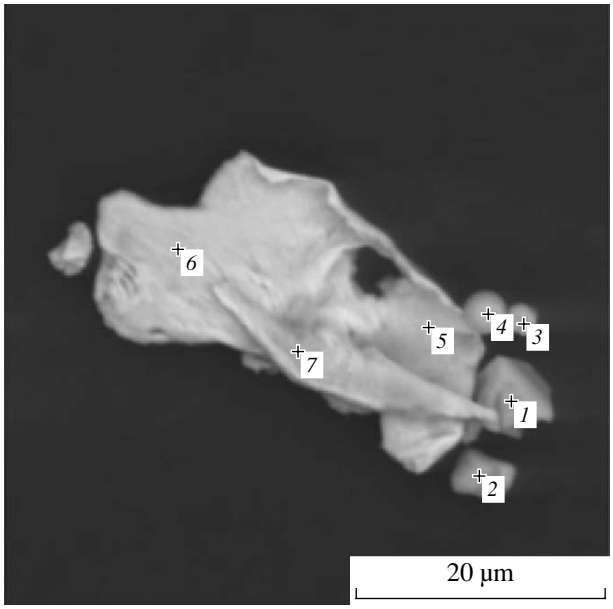

Grain	O	Mg	Al	Si	S	Cr	Mn	Fe	Ni	Mo
2	23.65	4.08	2.04			4.71		59.49	6.02	
3	15.21							84.79		
4	37.70	9.11	2.99			5.64		41.82	2.74	
5	30.23	5.78	2.73			5.55		51.32	4.39	
6	39.28	1.56	0.67			0.45	1.23	50.26	6.56	
7				0.56			0.65	17.99	76.67	4.13
8	2.39		1.95	0.51				11.44	81.58	2.13
10	2.78			0.77	1.20		0.86	14.62	79.78	

Grain	O	Mg	Al	Si	Ca	Ti	Cr	Mn	Fe	Ni	Cu
1	31.65	4.53	1.40			0.34	3.21	0.93	54.39	3.54	
2	28.83	4.14	0.94	0.28	0.29		1.18	0.96	61.07	2.30	
3	31.87		0.61	0.58			1.26	1.51	59.41	4.76	
4	31.11		0.31					0.45	68.13		
5									99.30		0.70
6									100.00		
7	5.84		0.34	1.08				0.55	91.60		0.59

Fig. 4. (Contd.)

$J6_5$. TMA data point to the presence of magnetite with T_C = 590°C (~0.004%), hemoilmenite with T_C ~ 300°C (~0.05%), and iron with T_C ~ 700–750°C (extrapolation). The microprobe examination of the magnetic fraction revealed an Ni grain with taenite segregations. Such grains were not discovered in the TMA sample; i.e., these are isolated grains.

$J6_6$. According to TMA data, nickel with T_C = 350°C (~0.4%) and titanomagnetite with T_C = 520°C (~0.1%) are present. Such enrichment in Ni balls is local: except for isolated Ni lamellae similar to those shown in Fig. 1, they were found in none of the sample pieces adjacent to $J6_6$.

The main magnetic minerals present in boundary layers of the Gams-1A, -1B, -2A, and -2B sections are as follows.

Goethite (T_C ~ 100–180°C) occurs ubiquitously according to TMA and microprobe data (Fig. 2, Table 2). The goethite concentration varies almost in the same way as the paramagnetic magnetization (Fig. 3) in both Gams-1 [Pechersky et al., 2006] and Gams-2. The magnetic fraction often contains balls of goethite and hematite (Figs. 4, 5) that are evidently oxidation products of metallic iron balls; they are highly magnetic, which implies that metallic iron has quite probably been preserved at their centers.

Ni-bearing ferrospinels (T_C = 100–150°C) are present in several samples from the Gams-1 and -2 boundary layers. At all the levels of the Gams-1A boundary layer and in the lower and middle parts of the Gams-2B layer, crystals of chrome spinel and Ni-bearing ferrospinel of a complex composition were discovered in the heavy and magnetic fractions (Figs. 4, 5) [Grachev et al., 2007]. The chrome spinel is distinguished by a high concentration of Cr_2O_3 (from 57 to 79%) and significant variations in MgO (3–20%) and FeO (13–40%). Spinel of such a composition is not ferromagnetic. The Ni-bearing ferrospinel (Figs. 4, 5) is most likely magnetic. It is evident that precisely this ferrospinel (at least some of its grains with FeO ≥ 60%) is a source of magnetization with T_C = 100–150°C. The amount of these grains can significantly rise if an appreciable part of impurity elements in ferrospinel form "extrinsic" inclusions that do not contain iron or, on the contrary, inclusions are composed of magnetic ferrospinel. Ferrospinel is represented by octahedral crys-

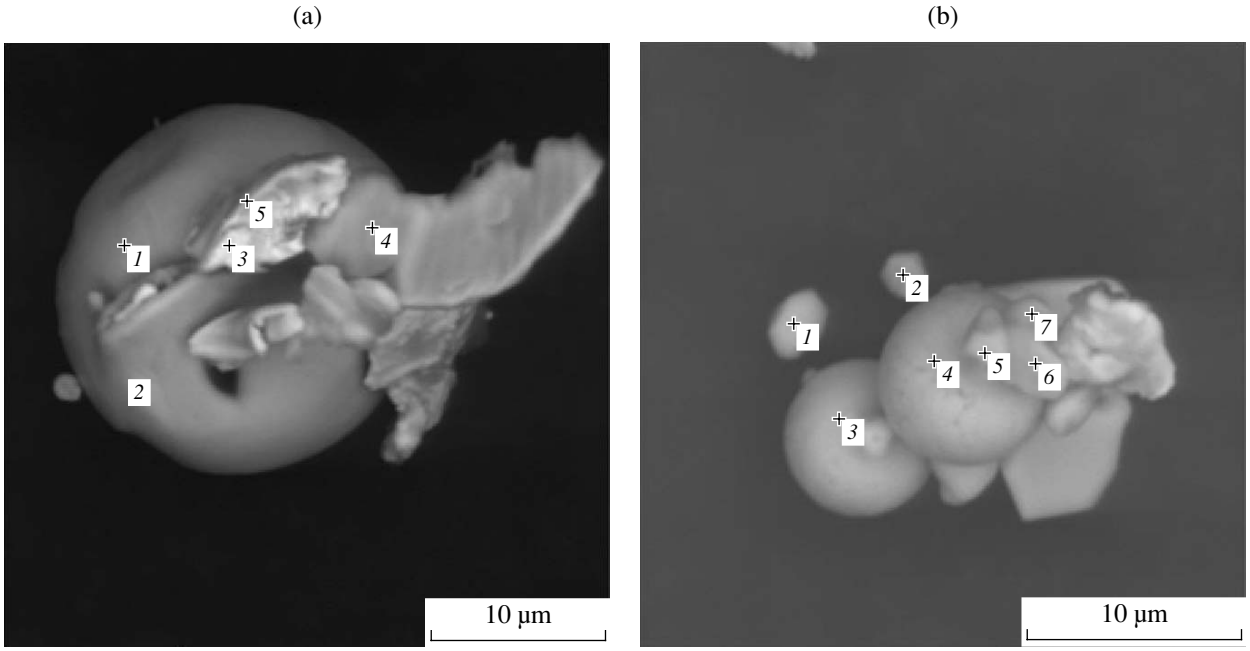

Grain	O	Al	Si	S	Ca	Fe	Zn
1	36.08					63.92	
2	34.55					65.45	
3	5.85		1.58	1.15		84.28	7.14
4						100.00	
5	6.49	0.55	1.89		0.44	84.97	5.65

Grain	O	Mg	Al	Si	Cr	Mn	Fe	Ni
1	34.63	3.11	1.29		3.99	1.62	52.00	3.36
2	34.95	4.25	1.13		4.39	0.87	50.20	4.22
3	35.00						65.00	
4	35.10						64.90	
5	38.06	4.40	1.24	0.73	2.09		50.51	2.98
6	33.46	6.82	1.67		4.77		47.93	5.35
7	42.34	8.37	2.74	2.31	4.07		34.63	5.54

Fig. 5. Examples of goethite and hematite balls from the lower part of the Gams-2 boundary layer: (a) ball of goethite with hematite from metallic iron (*1*, *2*) and iron lamellae, pure (4) and with impurities and inclusions (*3*, *5*); (b) balls of goethite with hematite from metallic iron (*3*, *4*) and fine crystals of Ni-bearing ferrospinel (*1*, *2*, *5*, *6, 7*).

tals up to 10–15 μm in size (Figs. 4, 5) because its sources are not far off. As seen from Figs. 4 and 5, sharp uncorrelated fluctuations in admixture concentrations are characteristic of the Ni-bearing ferrospinel composition. This is quite explicable due to the presence of microinclusions of other minerals in ferrospinel. Such differences in the composition of the Ni-bearing ferrospinel grains, which are very close in the time and place of their deposition, and their very good preservation suggest, on the one hand, that their sources are different and, on the other hand, that the grains are close to the sources or, more specifically, that they have not experienced long-term reworking during their deposition. The combination of these facts implies that *cosmic dust* is the most probable source of these grains.

Hemoilmenite (T_C = 200–300°C), according to TMA data, is often present in samples from the boundary layer and is observed in the form of fine segregations in ilmenite grains that are products of ilmenite oxidation [Grachev et al., 2005; Pechersky et al., 2006]. According to data of microscopic and microprobe observations, the boundary layer contains a noticeable amount of ilmenite grains (Fig. 6) including altered grains with evidence of iron removal and hydration (Table 3).

Titanomagnetite (T_C = 400–530°C), according to both MTA and microprobe data, is fixed ubiquitously in thin sections and in heavy and magnetic fractions (Figs. 7a, 7b; Table 1); its along-section distribution is irregular (Fig. 2) but its composition is very similar in the Gams-1 and -2 sections (Tables 1a, 1b). The electron beam strikes either the titanomagnetite matrix (TiO_2 = 8–16%, Table 1) or ilmenite lamellae (TiO_2 = 29–34%, Table 1) that are, as a rule, noticeably smaller in size than the microprobe (~2 μm). This is the main cause of the fluctuations in the composition of grains measured by the microprobe. In all cases, the titanomagnetite compositions given in Table 1 correspond to calculated Curie points below 400°C, and the average

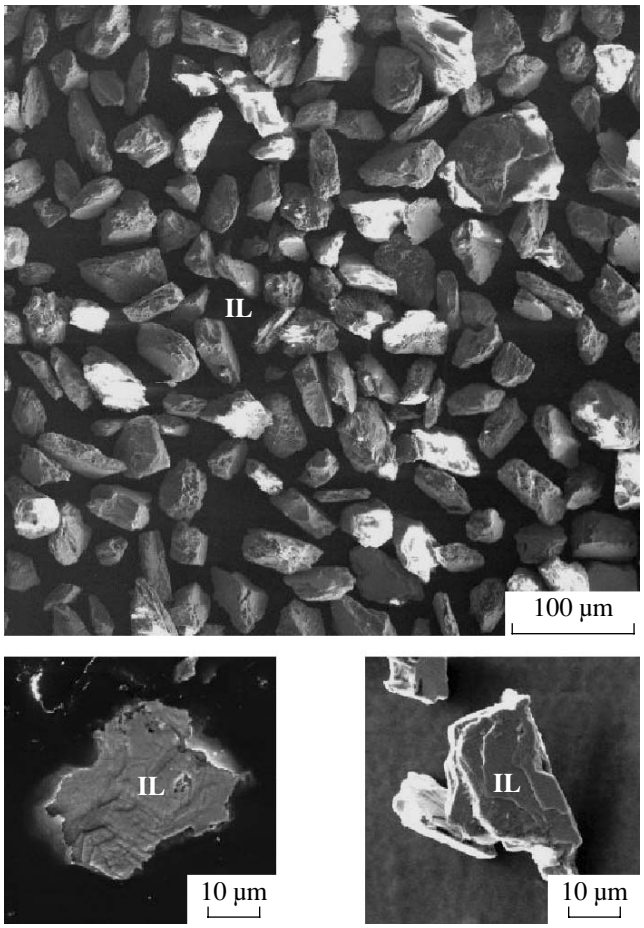

Fig. 6. Examples of ilmenite grains from the Gams boundary layer.

concentration $TiO_2 \approx 15\%$ correspond to $T_C \approx 300°C$, which is below the measured values and points unambiguously to decomposition of titanomagnetite grains measured by the microprobe. This is corroborated by an example of a decomposed titanomagnetite grain in a thin section (Fig. 7b). The average concentration $TiO_2 \approx 15\%$ is smaller than the typical averages of rift and spreading basalts ($TiO_2 \approx 20$–25%), whose grain composition is uniformly stable [Pechersky and Didenko, 1995; Pechersky et al., 1975]. On the other hand, titanomagnetite grains present at the base of the Gams-1A boundary layer ($J6_1$, Table 1) are typical of rift and similar basalts.

The main distinction of titanomagnetites of the Gams-1 and -2 boundary layers from titanomagnetites crystallizing in basaltic melts of different types is an *unusually small concentration of admixtures* (Table 1). Apparently, this specific pattern reflects the formation of titanomagnetite crystals from a *volcanic aerosol.*

Burov [2004] notes an abrupt rise in the magnetization of sediments caused by their enrichment in ash material beginning from the Permian/Triassic boundary, which reflects the global high volcanic activity at that time. It is very likely that a similar volcanic situation took place at the Mesozoic/Cenozoic boundary, producing a volcanic aerosol that contained titanomagnetite without admixtures.

Magnetite (T_C = 570–590°C) is fixed ubiquitously from TMA data (Fig. 2). The compositions of many magnetite grains from the Gams-1 boundary layer were measured with a microprobe (Table 4). As distinct from titanomagnetites, they often include grains containing noticeable admixtures of Mg, Al, Mn, and Cr. Evidently, these are primary magmatic crystals. Beyond the boundary layer, the Danian Gams-1 sediments are dominated by well-preserved single crystals of pure magnetite (Table 5; Figs. 7c, 7d, 7e) having evidently the same origin as the pure titanomagnetites (see above). Magnetic fractions contain balls of magnetite, hematite, and goethite (Figs. 4, 5) that have likely formed due to oxidation of metallic iron balls.

Metallic nickel ($T_C \approx 360°C$) and its alloy with iron. Virtually pure nickel was found in pieces of the sample *J*6 ($J6_4$ and $J6_6$) from the upper part of the Gams-1A boundary layer (see above and [Grachev et al., 2008]); this nickel occurs in the form of balls

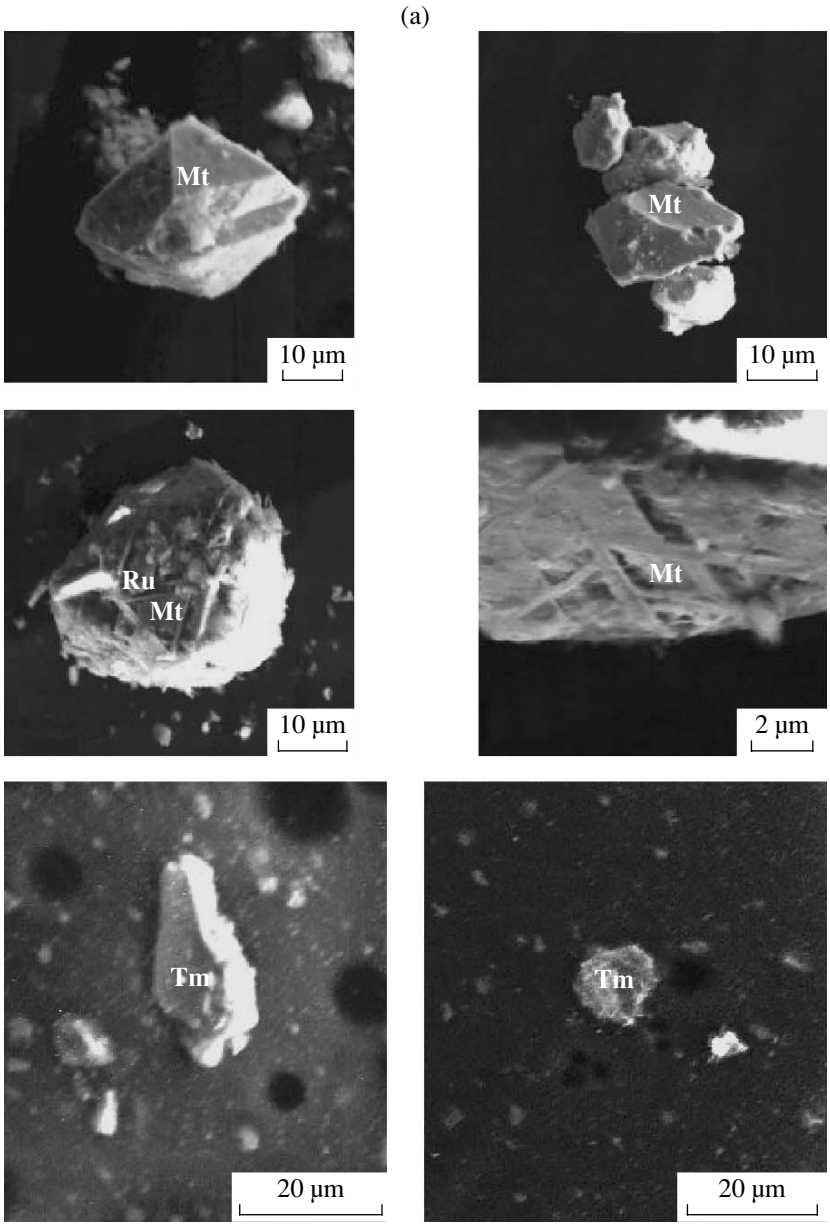

Fig. 7. (a) Examples of magnetite and titanomagnetite grains from the boundary layer (Gams-1 and Gams-2); (b) octahedron of magnetite covered with iron hydroxide (*1*) and a Ni-bearing ferrospinel grain (*2*); (c) octahedron of pure magnetite (*1*, *2*) and fine crystals of ferrospinel (*3*) and Ni-bearing ferrospinel (*4*); (d) pure magnetite grain and grains of weakly oxidized iron (*1*, *2*).

($J6_6$) and lamellae ($J6_4$). According to TMA and microprobe data, grains of Fe–Ni alloy with T_C = 640–660°C approximately corresponding in the proportion Fe/Ni to the formula Fe_3Ni (i.e., this is taenite) are also present there at various levels. Unlike the Gams-1A section, peculiarly shaped particles of a Ni–Fe–Mo alloy are found in the lower part of the Gams-2B boundary layer and more rarely in its middle part (Fig. 8) [Grachev et al., 2008]; they have Ni/Fe ≈ 5–6 and, therefore, are close in composition to awaruite. Such a ratio corresponds to Curie points of 410–430°C, but such a phase was not discovered from TMA data in the Gams-1 and -2 boundary layers, probably due to an irregular distribution of grains of this alloy (see section 2). Nickel and taenite balls of the Gams-1A type were not found in Gams-2.

Thus, we may state that, first, the Gams-1A nickel particles are homogeneous in composition and evidently formed from the same body (a meteorite); the Gams-2 awaruite particles are homogeneous in composition and, accordingly, also might have formed from the same body (a meteorite); however, both groups of particles significantly differ in composition and, there-

(b)

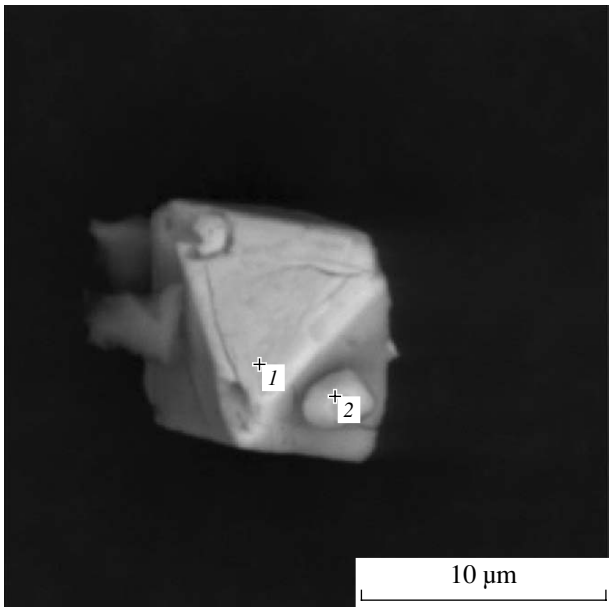

Grain	O	Mg	Al	Si	Cr	Fe	Ni	Zn
1	36.61		0.60	1.44		61.34		
2	37.00	3.89	1.31	0.54	2.52	48.98	3.22	2.55

(c)

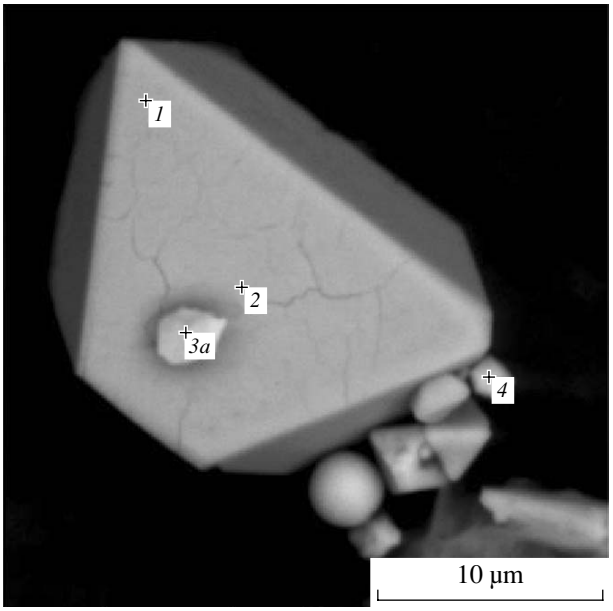

Grain	O	Mg	Al	Si	Cr	Fe	Ni	Zn
1	28.90					71.10		
2	28.69					71.31		
3	34.47		1.15	2.05		62.33		
4	33.74	3.64	0.89	0.87	2.01	49.96	6.82	2.08
3a	35.56		1.34	2.52		60.58		

(d)

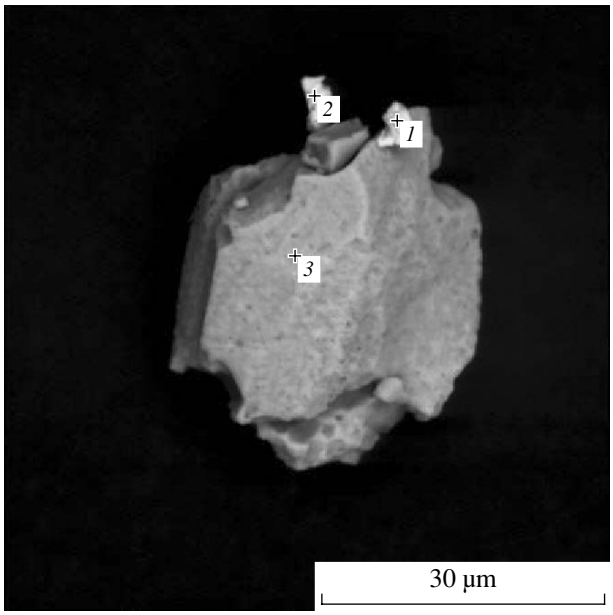

Grain	O	Al	Si	Cr	Fe
1	5.79	0.53			93.69
2	9.66		0.93	0.41	89.00
3	26.17				73.83

Fig. 7. (Contd.)

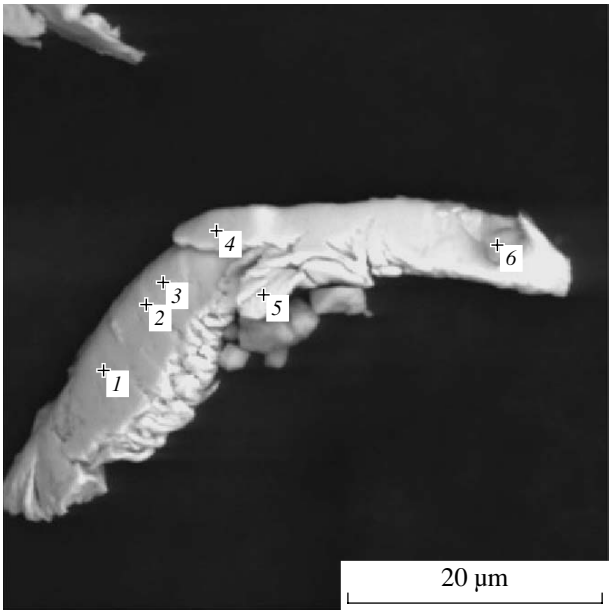

Mn	Fe	Ni	Mo
0.77	14.96	78.69	4.91
0.80	15.13	77.69	5.70
0.95	14.36	78.39	5.44
0.69	13.84	79.42	5.22
0.87	14.24	77.03	4.67

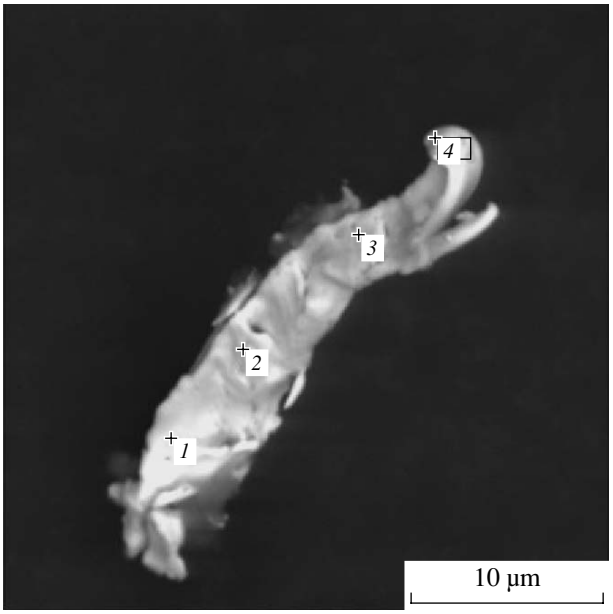

Grain	O	Al	Si	S	Mn	Fe	Ni	Mo
1	2.09		0.67	1.30	0.93	14.85	80.17	
2	4.25	0.48			0.96	15.58	77.55	1.18
3	4.29		1.11		0.81	13.14	76.15	4.50
4	7.67		0.93		1.01	12.90	73.55	3.94

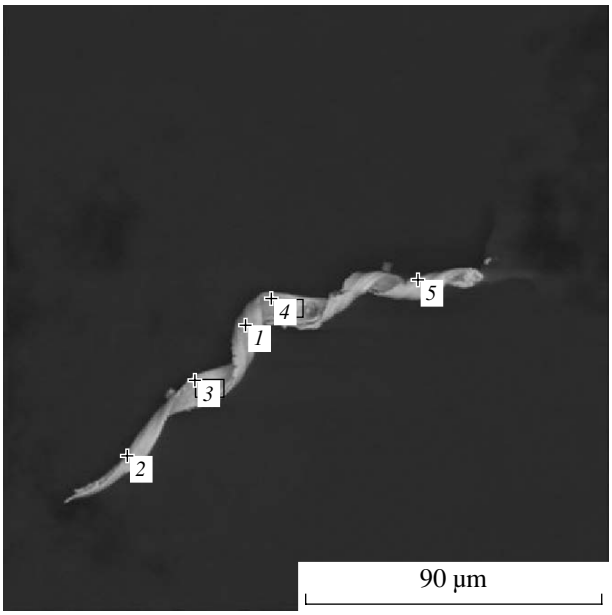

Grain	O	Si	Mn	Fe	Ni	Mo
1	2.90	0.61	0.86	13.21	77.86	4.56
2	2.10		0.67	13.64	80.86	2.73
3	2.94	0.59	0.70	14.48	77.09	4.20
4	1.90	0.46	0.74	14.19	80.05	2.67
5	2.83	0.59		13.92	78.10	4.55

Fig. 8. Examples of peculiarly shaped particles of Ni–Fe–Mo alloy (awaruite) from the lower part of the Gams-2B boundary layer.

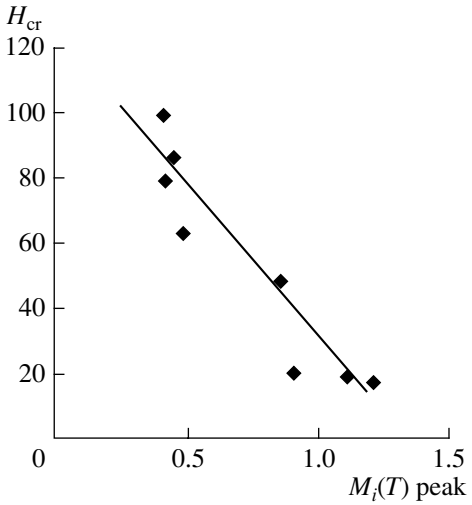

Fig. 9. Correlation between the peak height of the TMA curve and H_{cr} (Gams-2A and Gams-2B).

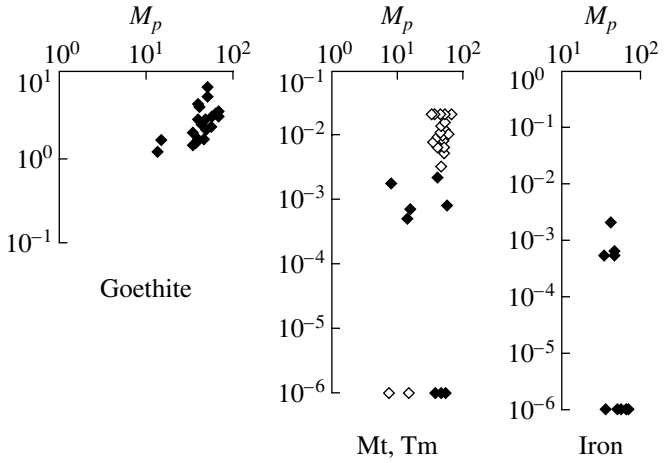

Fig. 10. Correlation between the paramagnetic magnetization and the percentage concentrations of goethite, magnetite, titanomagnetite (open circles), and metallic iron in the boundary layer (Gams-1 and Gams-2).

fore, should be related to different meteorites. Second, Gams-1 and Gams-2 particles differ in time: the former are located in the upper part of the boundary layer (Gams-1), and the latter in the lower part (Gams-2). In other words, these particles belong to meteorites of different ages and are associated with different *local impact events.*

Metallic iron (T_C = 750–770°C) is present in small concentrations (<0.001%) in the Danian and Maastrichtian deposits but is found solely in the form of separate grains in the Gams-1 boundary layer [Pechersky et al., 2006; Grachev et al., 2008]. In the Gams-2A and Gams-2B boundary layers, it is discovered only in their lower parts and, in the Gams-1B layer, only in its upper part (Fig. 2). The Gams-2B particles of metallic iron occur generally in the form of lamellae etc. (Fig. 4) and more rarely in the form of balls; the particles are often covered with iron hydroxides and/or altered to magnetite and hematite (Figs. 4, 5).

"Pyrite." As distinct from Gams-1, the Gams-2A and Gams-2B boundary layers yield a peak at 540 ± 5°C in the TMA curves. The peak is highest at the base of the boundary layers and regularly decreases toward the Danian deposits, where it almost disappears. After the peak, the TMA curves drop to zero at a Curie point of 590–595°C; i.e., laboratory heating leads to the formation of magnetite, which oxidizes to hematite during the subsequent heating of a sample to 800°C. The peak masks appreciably the interval 500–600°C; this is why natural magnetite, often found in Gams-1 samples (where its concentration varies from 0 to 0.01–0.02%) [Pechersky et al., 2006], is unrecognizable in the first heating TMA curves from Gams-2A and Gams-2B rocks. Indirect evidence of the presence of magnetite in Gams-2A is the negative correlation of the remanent coercivity H_{cr} measured before heating (i.e., before the formation of magnetite) with the TMA peak height (Fig. 9). The magnetite formation during laboratory heating is related to the fact that boundary layer samples contain Fe sulfides such as pyrite, which were noted in the layer from mineralogical observations. The amount of the newly formed magnetite evidently reflects the amount of "pyrite," implying that the magnetization of the newly formed magnetite can provide constraints on the lower bound of the possible "pyrite" concentration in a sample (Fig. 2).

A clear positive correlation between the M_p value and the goethite concentration is observed both in all the sediments studied [Pechersky et al., 2006] and in the boundary layer (Fig. 10). On the other hand, the concentrations of magnetite, titanomagnetite, and metallic iron do not correlate with the concentration of iron hydroxides (Fig. 10). This indicates independent conditions of accumulation of these minerals and, evidently, their different sources.

4. CONCLUSIONS

(1) The boundary layers in the Gams-1 and Gams-2 sections differ in the composition and along-section position of metallic nickel and its alloy with iron: compositionally homogeneous pure metallic nickel is present in the upper part of the Gams-1 section, and taenite is found in different parts of the section; in the Gams-2 section, pure nickel is absent and a compositionally homogeneous Ni–Fe–Mo alloy (awaruite) is present at the base of the layer. Therefore, accumulations of nickel and awaruite particles are associated with falls of different small meteorites at different times. The effect of these falls is local and is not felt at a distance of about 0.5 km (the distance between Gams-1 and Gams-2).

(2) Particles of metallic iron are very rare in the boundary layer. They are noted in the upper and lower parts of the Gams-1 layer and in the lower part of the

Gams-2 layer. Considering that, except the boundary layer, metallic iron particles are spread ubiquitously, at least in all of the studied sections including the K/T boundary, and their distribution in time is rather random, it is most likely that the source of the majority of the metallic iron particles is cosmic dust.

(3) Ni-bearing ferrospinel is present all along the boundary layer, and its composition varies within wide limits. The well-preserved shape of its crystals is evidence for nearby sources of ferrospinel grains and/or their rapid delivery into the sediment, for example, from the atmosphere, cosmic dust, and so on. It is natural to suggest that cosmic dust was the source of compositionally so heterogeneous Ni-bearing ferrospinel that arose at the same time and in the same place. Inclusions of Ni-bearing ferrospinel grains are met in particles of metallic iron and awaruite, indicating that they or at least some particles of both types have a common origin.

(4) The lower part of the Gams-1 boundary layer is characterized by a noticeable enrichment in titanomagnetite with a Ti concentration typical of rift and plume basalts. This phenomenon is not observed in the lower part of the Gams-2A layer. The titanomagnetite concentration varies in the latter within narrow limits (0.01–0.02%) and is even lower at the base of the Gams-2B layer. This suggests that the deposition of the titanomagnetite particles was very irregular in both space and time. It is noteworthy that, in both sections except the lower Gams-1A, the composition of titanomagnetites is very homogeneous, with their Ti concentration being appreciably smaller than in rift and plume basalts.

All titanomagnetites of Gams-1 and Gams-2 typically have very low concentrations of impurities as compared with usual values in titanomagnetites of igneous rocks, where they generally attain a few percent. This distinction is possibly due to crystallization of the titanomagnetites from a volcanic aerosol.

(5) As distinct from titanomagnetites, many grains of magnetite from the boundary layer are characterized by higher concentrations of impurities. Possibly, impurity magnetites are primary magmatic products of acidic magmatism. Apart from this variety, well-preserved crystals of pure magnetite, evidently of nonmagmatic origin, are present in both the boundary layer and Danian deposits. The good preservation of the crystals is evidence for close sources of their accumulation in the sediments.

(6) Pyrite is present in the Gams-2 boundary layer but is not discovered in the Gams-1 section. Its concentration is highest at the base of the boundary layer and regularly decreases upward along the section. Fe sulfides are absent in the Danian deposits above the boundary layer. We suggest that the magnetite formed from the sulfides is responsible for the low coercivity of sediments in the lower part of the boundary layer in Gams-1 and Gams-2.

(7) The concentration of iron hydroxides follows the same variation pattern: it is lowest at the very base of the boundary layer and continuously increases to a maximum at a level of ~10 mm, after which it gradually decreases. As a result, sediments are sharply enriched in iron hydroxides at the K/T boundary. This is a global effect [Pechersky, 2008] unrelated to local physiographic features of accumulation of terrigenous material in the sediments. Apparently, the accumulation patterns of the bulk of iron hydroxides in the boundary layer and other deposits were different: in the former case, the mechanism of their accumulation was common to all sediments of the boundary layer (for example, a kind of metalliferous sediments) and independent of the local conditions, while, in the latter case, they are of a volcanic–terrigenous origin depending on local conditions. The absence of correlation of magnetite, titanomagnetite, and metallic iron concentrations with iron hydroxides is evidence for different sources of their accumulation in the boundary layer.

Thus, only *the enrichment in iron hydroxides of a common (hydrothermal?) origin can be considered as a global consistent phenomenon associated with the K/T boundary.* Such a phenomenon cannot be an impact event.

REFERENCES

1. B. V. Burov, "Boundary between the Permian and Triassic Rocks in the Moscow Syneclise Reconstructed from the Rock Sequences Exposed in the Kichenenga River Basin," Russ. J. Earth Sci. **7** (2) (2004).
2. A. F. Grachev, O. A. Korchagin, H. A. Kollmann, et al., "A New Look at the Nature of the Transitional Layer at the K/T Boundary near Gams, Eastern Alps, Austria, and the Problem of the Mass Extinction of the Biota," Russ. J. Earth Sci. **7** (6) (2005).
3. A. F. Grachev, V. A. Tselmovich, O. A. Korchagin, and H. A. Kollmann, "Two Spinel Populations from Cretaceous–Paleogene Boundary Clay Layer in the Gams Stratigraphic Sequence, Eastern Alps," Russ. J. Earth Sci. **9** (2007).
4. A. F. Grachev, O. A. Korchagin, V. A. Tselmovich, and H. A. Kollmann, "Cosmic Dust and Micrometeorites in the Transitional Clay Layer at the Cretaceous–Paleogene Boundary in the Gams Section (Eastern Alps): Morphology and Chemical Composition," Fiz. Zemli, No. 7 (2008) [Izvestiya, Phys. Solid Earth **44** (7) (2008)].
5. R. Lahodynsky, "Lithostratigraphy and Sedimentology across the Cretaceous/Tertiary boundary in the Flyschgosau (Eastern Alps, Austria)," Riv. Espanola de Paleontologia, N° Extraordinario, 73–82 (1988).
6. D. M. Pechersky, "Enrichment of Sediments in Iron Hydroxides at the Mesozoic-Cenozoic Boundary: A Synthesis of Petromagnetic Data," Fiz. Zemli, No. 3, 65–72 (2008) [Izvestiya, Phys. Solid Earth **44**, 232–238 (2008)].
7. D. M. Pechersky et al., *Magnetism and Formation Conditions of Igneous Rocks* (Nauka, Moscow, 1975) [in Russian].
8. D. M. Pechersky and A. N. Didenko, *Paleo-Asian Ocean* (OIFZ RAN, Moscow, 1995) [in Russian].
9. D. M. Pechersky, A. F. Grachev, D. C. Nourgaliev et al., "Magnetolithologic and Magnetomineralogical Characteristics of Deposits at the Mesozoic/Cenozoic Boundary: Gams Section (Austria)," Russ. J. Earth Sci. **8** (3) (2006).